Chinese Chemical Letters 37 (2026) 111589

Contents lists available at ScienceDirect

Chinese Chemical Letters

journal homepage: www.elsevier.com/locate/cclet

A hypoxia-activated photothermal agent suppressing thermotolerance and secondary inflammation for enhanced tumor ablation

Kaiye Wang[1], Yuting Jia[1], Xiaohan Liu, Wei Pan, Xiuyan Wan, Na Li*, Bo Tang

College of Chemistry, Chemical Engineering and Materials Science, Key Laboratory of Molecular and Nano Probes, Ministry of Education, Collaborative Innovation Center of Functionalized Probes for Chemical Imaging in Universities of Shandong, Institute of Molecular and Nano Science, Shandong Normal University, Ji'nan 250014, China

ARTICLE INFO

Article history:
Received 12 May 2025
Revised 14 July 2025
Accepted 15 July 2025
Available online 17 July 2025

Keywords:
Photothermal therapy
Mitochondrial targeting
Heat shock protein inhibition
Inflammation suppression
Hypoxia-activation

ABSTRACT

Developing effective strategies to simultaneously suppress tumor thermotolerance and secondary inflammation remains a significant challenge in enhanced photothermal therapy (PTT). In this study, we developed a nitroreductase (NTR)-triggered multifunctional photothermal agent (m-SCy-DCF) by conjugating mitochondria-targeted sulfur-substituted hemicyanine to the anti-inflammatory diclofenac (DCF) through an NTR-cleavable linker. Upon activation in the hypoxic tumor microenvironment, m-SCy-DCF selectively accumulated in mitochondria and generated localized hyperthermia under laser irradiation. This process not only disrupted mitochondrial function but also suppressed the expression of heat shock proteins (HSPs). Simultaneously, the released DCF exerted potent anti-inflammatory effects, effectively reducing the levels of inflammatory cytokines *in vivo*. This dual suppression of tumor thermotolerance and inflammation induced immunogenic cell death and achieved effective tumor ablation, demonstrating the potential of m-SCy-DCF as a highly promising candidate for enhanced PTT.

© 2026 Published by Elsevier B.V. on behalf of Chinese Chemical Society and Institute of Materia Medica, Chinese Academy of Medical Sciences.

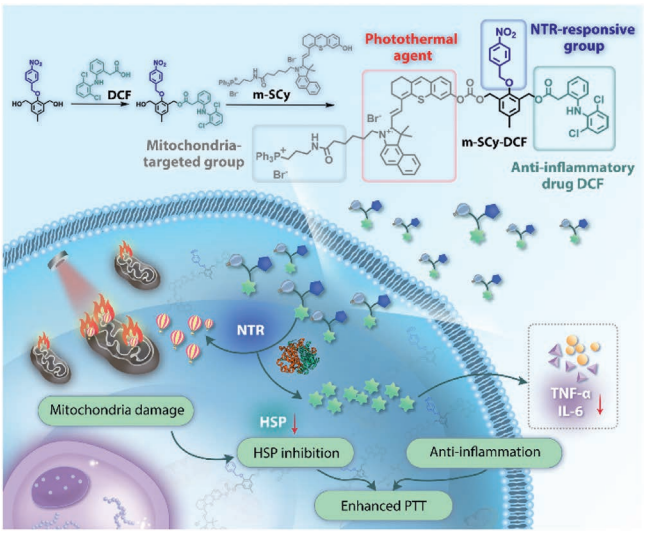
Photothermal therapy (PTT), characterized by its non-invasive property and high specificity, has garnered considerable attention in the field of cancer therapy [1–5]. Distinct from conventional treatments, PTT utilizes harmless near-infrared light as an energy source to induce localized hyperthermia, thereby triggering cell apoptosis or necrosis for effective tumor ablation [6,7]. PTT has exhibited superior spatiotemporal controllability through precise modulating light intensity and exposure duration, as well as meticulously designing tumor-targeted photothermal agents, which provides great prospect in precise tumor therapy [8,9].

Although PTT holds significant potential for tumor ablation, several challenges remain to be addressed to enhance therapeutic efficiency and improve prognosis. One major challenge is the cellular protective response to hyperthermic stress, which is characterized by the rapid induction of heat shock proteins (HSPs) [10,11]. These chaperone proteins play a crucial role in repairing hyperthermia-induced cellular damage, thereby increasing the thermotolerance of cells and reducing the efficacy of PTT [12]. Given the substantial energy chaperone associated with the transcription and translation of upregulated HSPs, therapeutic strategies aimed at inhibiting cellular metabolism have shown great promise in mitigating these limitations [13–15]. Targeting and disrupting mitochondrion, the well-known powerhouse in cell, represents a prominent approach to inhibiting the upregulation of HSPs [16–18]. In addition, PTT-induced secondary inflammatory response poses another notable challenge in tumor therapy [19,20]. Located hyperthermia causes cytoplasmic membrane disruption and the release of damage-associated molecular patterns, which promotes the inflammatory response within tumor tissues. Excessive inflammation elevates the risk of tumor metastasis and recurrence, subsequently impairing the overall therapeutic outcome [21–23]. Therefore, simultaneously inhibiting HSP-mediated thermotolerance and suppressing the secondary inflammatory response is anticipated to significantly enhance the efficacy of PTT.

Utilizing over-expressed markers in tumor tissues to activate therapeutic agents represents a promising strategy, which substantially minimizes off-target effects on surrounding healthy tissues [24–27]. Given the characteristics of rapid proliferation, intense metabolic activity, and aberrant angiogenesis of tumor tissue, tumor cells usually reside in a hypoxic microenvironment [28]. Consequently, the level of nitroreductase (NTR) is significantly upregulated, which potentially serves as an effective trigger for PTT agents [29,30]. Herein, we designed and synthesized an NTR-triggered photothermal agent (designated as m-SCy-DCF) with anti-inflammatory and HSP-inhibitory functions for effective

* Corresponding author.
E-mail address: lina@sdnu.edu.cn (N. Li).
[1] These authors contributed equally to this work.

https://doi.org/10.1016/j.cclet.2025.111589
1001-8417/© 2026 Published by Elsevier B.V. on behalf of Chinese Chemical Society and Institute of Materia Medica, Chinese Academy of Medical Sciences.



Scheme 1. The synthesis of multifunctional photothermal agent m-SCy-DCF and the schematic diagram of enhanced PTT efficacy through suppressing thermotolerance and secondary inflammation.

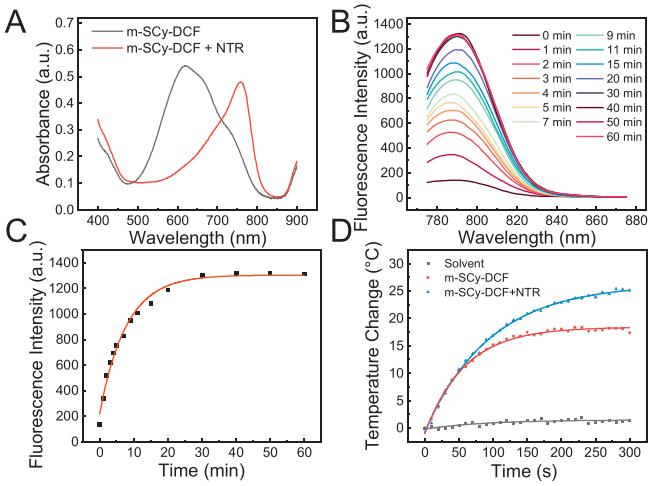


Fig. 1. (A) The ultraviolet–visible absorption spectra of m-SCy-DCF (30 μmol/L) treated with/without NTR (1 μg/mL). The changes in fluorescence intensity (B) and related quantization (C) of m-SCy-DCF over time after incubation with NTR (1 μg/mL). Ex = 756 nm. (D) Temperature changes of m-SCy-DCF (300 μmol/L) with/without NTR (10 μg/mL) upon 750-nm laser irradiation (0.6 W/cm^2, 5 min).

PTT. The selective activation of m-SCy-DCF by NTR enabled the localized release of photothermal agent specifically within malignant tissue, which was expected to protect normal tissues from thermal damage and enhance the safety of the treatment. To construct the multifunctional photothermal agent m-SCy-DCF, mitochondria-targeted sulfur-substituted hemicyanine (m-SCy) was conjugated to the anti-inflammatory diclofenac (DCF) *via* NTR-cleavable linkers. Within hypoxic microenvironment, NTR catalyzed the conversion of nitro groups into amino groups, triggering a cascade of electronic restructuring and the subsequent liberation of m-SCy and DCF (Scheme 1). The activated m-SCy selectively accumulated within mitochondria and generated localized hyperthermia under laser irradiation to directly damage mitochondria, thereby cutting off the energy supply and inhibiting the expression of HSPs. The released DCF, serving as a non-steroidal anti-inflammatory drug (NSAID), exhibited significant efficacy in relieving hyperthermia-caused secondary inflammation. The experimental results showed that m-SCy-DCF localized mitochondria and reduced HSP expression under laser irradiation. Furthermore, it effectively curtailed the levels of inflammatory cytokines *in vivo*, thereby exerting a profound inhibitory effect on tumor growth.

The multifunctional photothermal agent m-SCy-DCF was synthesized following the synthetic route outlined in Fig. S1 (Supporting information). In brief, 4-nitrobenzyl bromide was introduced to afford the key intermediate compound **1**, endowing m-SCy-DCF with NTR-responsive property. Subsequently, the anti-inflammatory drug DCF was esterified with compound **1** *via* an ester linkage to form compound **2**. Finally, the mitochondrion-targeted photothermal agent m-SCy was coupled through an activation process mediated by *p*-nitrophenyl carbonate, yielding the desirous photothermal agent m-SCy-DCF. Nuclear magnetic resonance (NMR) spectroscopy and high-resolution mass spectrometry (HRMS) were employed to confirm the structural integrity of m-SCy-DCF and related intermediates (Figs. S2–S7 in Supporting information). The detailed analysis of the corresponding spectra validated the precise molecular structures and successful synthesis of the designed compound.

The NTR-mediated release of photothermal molecules and DCF was determined preferentially. The absorbance of m-SCy-DCF solution exhibited a significant decrease within the 500–700 nm range upon incubation with NTR, while it increased observably in the range from 700 nm to 800 nm (Fig. 1A). The redshift of the absorption wavelength is conducive to the photothermal conversion in the near-infrared region. Fluorescence spectroscopy was also utilized to monitor the release of active molecules. As illustrated in Figs. 1B and C, upon incubation with NTR, the fluorescence intensity at 790 nm progressively increased over time and reached a plateau within approximately 30 min, indicating that the active molecules were effectively released within a short time. Additionally, high-performance liquid chromatography (HPLC) analysis confirmed the successful release of the active photothermal agent m-SCy from m-SCy-DCF following NTR treatment (Fig. S8 in Supporting information). Next, the photothermal conversion performance was tested by recording the temperature changes with a thermal imager. As shown in Fig. 1D and Fig. S9 (Supporting information), the temperature of the solution increased by 25 °C in the presence of NTR under laser irradiation (750 nm, 0.6 W/cm^2), while the group without NTR increased by only 15 °C. These results demonstrated that m-SCy-DCF could be effectively activated by NTR and held significant potential for tumor PTT. Subsequently, the concentration of m-SCy-DCF and the laser power density were adjusted to further study the photothermal conversion effect. As shown in Fig. S10 (Supporting information), the temperature changes increased with the increasement of concentration and power density. To ensure the sustained efficacy of PTT in eliminating tumor cells, a laser power density of 0.6 W/cm^2 was selected for subsequent experiments. The stability of the photothermal agent was further evaluated *via* a heating and cooling cycle experiment (Fig. S11 in Supporting information). It was concluded that m-SCy exhibited satisfactory photothermal stability, as the temperature still increased to 50 °C after three cycles of laser switching. These results indicated that m-SCy-DCF could be efficiently activated by NTR to generate hyperthermia under laser irradiation for tumor ablation.

Subsequently, cell viability was investigated under hypoxic and normoxic conditions to assess the cytotoxic effects of m-SCy-DCF. As shown in Fig. S12 (Supporting information), cells maintained high viability upon exposure to various concentrations of m-SCy-DCF in the dark, independent of oxygen levels. However, a concentration-related decrease in cell viability occurred after laser irradiation, which was more pronounced under hypoxia, consistent with hypoxia-induced NTR upregulation (Fig. 2A). In addition, we systematically assessed the inhibitory effects on tumor cells in various groups, including the control group (Control), laser-irradiated group (Laser), DCF-treated group (DCF), m-SCy-treated group (m-

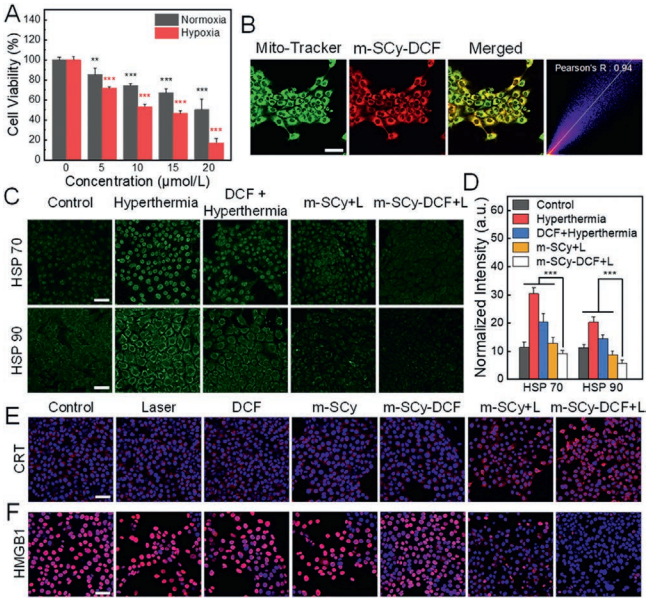


Fig. 2. (A) Cell viability of 4T1 cells incubated with different concentrations of m-SCy-DCF upon irradiation with a 750-nm laser (0.6 W/cm^2, 5 min). (B) The co-localized confocal fluorescence images of m-SCy-DCF (red) and commercial Mito-Tracker (green). Immunofluorescent images (C) and related quantification (D) of HSP 70 and HSP 90 under various conditions. The levels of typical ICD markers CRT (E) and HMGB1 (F) in 4T1 cells under different treatments. Scale bar: 50 μm. $^{**}P < 0.01$, $^{***}P < 0.001$. n.s., no significance. Data are presented as mean ± standard deviation (SD) ($n = 3$).

SCy), m-SCy-DCF-treated group (m-SCy-DCF), and groups receiving additional laser irradiation (m-SCy+L and m-SCy-DCF+L). As depicted in Fig. S13 (Supporting information), the lowest cell viability was observed in m-SCy+L and m-SCy-DCF+L groups, implying superior tumor suppression. Live/dead cell staining assay revealed similar results, with a significantly higher proportion of PI-stained cells in the m-SCy+L and m-SCy-DCF+L groups compared to others, demonstrating the enhanced PTT capability of the photothermal agent (Fig. S14 in Supporting information). Cell migration and colony formation assays were conducted to verify the effects of different materials on cell motility and proliferation respectively (Figs. S15 and S16 in Supporting information). The scratch wounds in laser-treated groups (m-SCy+L and m-SCy-DCF+L) remained negligible changes, while those in control groups were closed in varying degrees. These results suggested that m-SCy-DCF exhibited a substantial capacity to inhibit cell migration following laser irradiation. Meanwhile, the obviously decreased colony number in the colony-formation experiment verified that cell proliferation was substantially inhibited in m-SCy-DCF+L group (Fig. S16). The above results demonstrated that m-SCy-DCF possessed significant cytotoxicity under laser irradiation and effectively suppressed the movement and proliferation of tumor cells.

Given the presence of the lipophilic triphenylphosphine group, it was hypothesized that the agent would preferentially localize to and damage the mitochondria. Colocalization images demonstrated a substantial overlap between the fluorescent signals of m-SCy-DCF and commercial mitochondrial localization dyes, yielding a calculated colocalization coefficient of 0.94 (Fig. 2B). Subsequently, the JC-1 probe was utilized to assess the changes in mitochondrial membrane potential (Fig. S17 in Supporting information). When incubated with m-SCy-DCF and exposed to laser irradiation, tumor cells exhibited a bright green fluorescence signal (JC-1 monomers) rather than a red signal (JC-1 aggregates), suggesting substantial decrease in membrane potential. Mitochondrial damage plays a critical role in inducing apoptosis, resulting in the upregulation of downstream caspase-3. The immunofluorescence staining images (Fig. S18 in Supporting information) confirmed the highest levels of caspase-3 were observed in the m-SCy-DCF+L group, indicating the most significant degree of apoptosis.

Next, the expression levels of HSPs in cells under various conditions were further explored. As illustrated in Figs. 2C and D, cells exposed to a high-temperature environment exhibited a significant stress response, leading to markedly elevated expression of HSP 70 and HSP 90. However, the groups targeted to mitochondria (m-SCy+L and m-SCy-DCF+L) exhibited a more pronounced reduction in HSP levels, likely attributable to hyperthermia-induced mitochondrial damage. Notably, the groups treated with DCF possessed a superior inhibitory effect on HSP, which was probably associated with the previously reported DCF-mediated inhibition of glucose transport [31]. Studies have demonstrated that PTT could cause immunogenic cell death (ICD) and trigger the release of tumor-associated immunogens, which further stimulates the immune system to attack tumor cells. Therefore, the expression of several ICD markers, such as calreticulin (CRT) and high-mobility group box 1 (HMGB1), was assessed in Figs. 2E and F. The results showed that the level of CRT significantly increased in m-SCy-DCF-incubated cells upon laser irradiation. Meanwhile, HMGB1 rapidly translocated from the nucleus to the extracellular space, resulting in a decreased fluorescence signal. These results indicated the successful induction of ICD.

In vivo experiments were then conducted and approved by the Animal Experiment Ethics Committee of Shandong Normal University (No. AEECSDNU2024068). The temperature changes in tumor areas were first recorded as shown in Fig. S19 (Supporting information). A significant increase was observed in the m-SCy-DCF+L group, reaching approximately 50 °C following irradiation. Building upon the efficacy of m-SCy-DCF in inhibiting tumor cell proliferation, we subsequently evaluated its anti-tumor potential *in vivo* using a tumor-bearing mouse model. The mice were divided into following groups: (I) control, (II) laser, (III) DCF, (IV) m-SCy, (V) m-SCy-DCF, (VI) m-SCy+L, and (VII) m-SCy-DCF+L. As shown in Figs. 3A and B, m-SCy-DCF+L group exhibited the most significant tumor growth suppression among all treatment modalities. These satisfactory results were attributed to the synergistic effects of thermal ablation, DCF-mediated inflammation relief, and the inhibition of HSPs.

To verify the anti-inflammatory effect of m-SCy-DCF *in vivo*, serum samples were collected 24 h post-treatment to determine the levels of inflammatory cytokines, such as tumor necrosis factor-α (TNF-α) and interleukin-6 (IL-6). As demonstrated in Figs. 3C and D, samples from m-SCy+L group exhibited a significant increase in inflammatory cytokines, indicating the occurrence of PTT-induced secondary inflammation. However, the introduction of DCF (m-SCy-DCF+L group) effectively mitigated the inflammatory response as the levels of inflammatory cytokines were recovered. In addition, a series of experiments were conducted to assess the biosafety of the multifunctional photothermal agent. The body weight of mice (Fig. 3E) remained stable during the treatment period. Moreover, no obvious abnormalities were observed in several liver and kidney function indicators (Fig. 3F), blood routine (Fig. 3G), and hematoxylin and eosin (H&E) staining images of major organs (Fig. S20 in Supporting information), demonstrating that different treatments had no significant systemic toxic side effects on the mice.

In summary, a multifunctional photothermal agent m-SCy-DCF was developed to overcome the limitations of conventional PTT in terms of thermotolerance and secondary inflammation. By leveraging hypoxia-responsive activation, m-SCy-DCF efficiently disrupted tumor cell mitochondria, inhibited HSP expression, and alleviated hyperthermia-induced inflammation. The agent demonstrated robust photothermal conversion efficiency, mitochondrial targeting

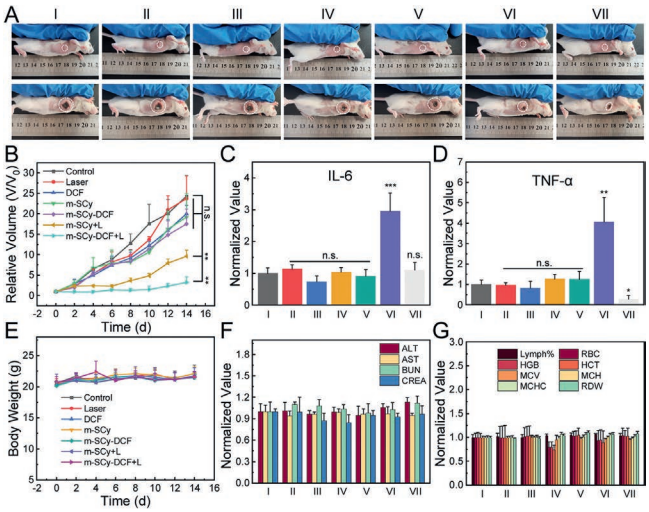


Fig. 3. (A) Photographs of mice under various treatments at day 0 and day 14. (B) Curves depicting changes in relative volume in different treatment groups. The levels of inflammatory cytokine IL-6 (C) and TNF-α (D) from the serum of mice in different treatment groups. (E) Body weight change curves for various treatment groups. Several indicators pertaining to liver and kidney function (F) and routine blood parameters (G) across different groups. $^{*}P < 0.05$, $^{**}P < 0.01$, $^{***}P < 0.001$. n.s., no significance. Data are presented as mean ± SD ($n = 3$). ALT, alanine aminotransferase; AST, aspartate aminotransferase; BUN, blood urea nitrogen; CREA, creatinine; HGB, hemoglobin; MCV, mean corpuscular volume; MCHC, mean corpuscular hemoglobin concentration; RBC, red blood cell count; HCT, hematocrit; MCH, mean corpuscular hemoglobin; RDW, red cell distribution width.

property, and ICD induction ability, resulting in significant tumor inhibition both *in vitro* and *in vivo*. Additionally, m-SCy-DCF exhibited excellent biosafety and effectively mitigated inflammatory responses, emphasizing its potential for clinical application in cancer therapy. This multifunctional platform represents a significant advancement in the field of PTT, offering a synergistic and safe strategy for enhancing therapeutic efficacy.

Declaration of competing interest

The authors declare that they have no known competing financial interests or personal relationships that could have appeared to influence the work reported in this paper.

CRediT authorship contribution statement

Kaiye Wang: Writing – original draft, Methodology, Conceptualization. **Yuting Jia:** Visualization, Investigation. **Xiaohan Liu:** Validation, Methodology. **Wei Pan:** Writing – review & editing, Supervision. **Xiuyan Wan:** Supervision, Funding acquisition. **Na Li:** Writing – review & editing, Supervision, Funding acquisition. **Bo Tang:** Writing – review & editing, Project administration.

Acknowledgments

This work was financially supported by the Natural Science Foundation of Shandong Province (Major Basic Research Project, No. ZR2023ZD44) and the Natural Science Foundation of Shandong Province (No. ZR2022YQ10).

Supplementary materials

Supplementary material associated with this article can be found, in the online version, at doi:10.1016/j.cclet.2025.111589.

References

[1] P. Xiao, W. Xie, J. Zhang, et al., J. Am. Chem. Soc. 145 (2023) 334–344.
[2] Y. Chen, S.Y. Yang, X. Ou, et al., J. Am. Chem. Soc. 146 (2024) 35462–35477.
[3] K. Wei, Y. Wu, X. Zheng, et al., Angew. Chem. Int. Ed. 63 (2024) e202404395.
[4] P. Chen, G. Zhang, J. Li, et al., Chem. Res. Chin. Univ. 40 (2024) 293–304.
[5] H. Kim, Y.R. Lee, H. Jeong, et al., Smart Mol. 1 (2023) e20220010.
[6] M. Overchuk, R.A. Weersink, B.C. Wilson, et al., ACS. Nano 17 (2023) 7979–8003.
[7] L. Li, X. Zhang, J. Zhou, et al., Small 18 (2022) 2107705.
[8] Y. Pu, W. Wu, B. Zhou, et al., Nano Today 44 (2022) 101461.
[9] Y. Ran, Z. Xu, M. Chen, et al., Adv. Sci. 9 (2022) 2200456.
[10] Z. Liu, S. Liu, L. Bin, et al., Angew. Chem. Int. Ed. 64 (2025) e202414879.
[11] S. Qin, H.Y. Zhao, X.Y. Luo, et al., ACS Nano 18 (2024) 32235–32254.
[12] F.H. Schopf, M.M. Biebl, J. Buchner, Nat. Rev. Mol. Cell Biol. 18 (2017) 345–360.
[13] J. Yang, Y. Zong, J. Su, et al., Nat. Commun. 8 (2017) 1201.
[14] Y. Bian, B. Liu, B. Ding, et al., Adv. Funct. Mater. 34 (2024) 2313853.
[15] L. Mei, Q. Ding, Y. Xie, et al., Biomaterials 315 (2025) 122968.
[16] S. Dong, Y. Dong, Z. Zhao, et al., J. Am. Chem. Soc. 145 (2023) 9488–9507.
[17] Y. Zhang, Z. Zhou, Z. Gao, et al., Chem. Eng. J. 474 (2023) 145677.
[18] Y. Dong, S. Dong, C. Yu, et al., Sci. Adv. 9 (2023) eadi9980.
[19] M. Shi, X. Liu, W. Pan, et al., J. Mater. Chem. B 11 (2023) 6478–6490.
[20] Y. Wang, K. Ma, M. Kang, et al., Chem. Soc. Rev. 53 (2024) 12014–12042.
[21] S.B. Coffelt, K.E. de Visser, Nature 507 (2014) 48–49.
[22] G. Wang, J. Li, L. Bojmar, et al., Nature 618 (2023) 374–382.
[23] S.W. Cole, J. Clin. Oncol. 27 (2009) 3418–3419.
[24] K. Wang, S.S. Xue, X. Liu, et al., Chem. Commun. 57 (2021) 6584–6595.
[25] Z. Wang, A. Wu, W. Cheng, et al., Nat. Commun. 14 (2023) 7251.
[26] S.Y. Wang, Y.H. Pan, Y.C. Qu, et al., Smart Mol. 2 (2024) e20230024.
[27] R. Wang, M. He, Z. Zhang, et al., Smart Mol. 2 (2024) e20240010.
[28] M.Z. Zou, W.L. Liu, H.S. Chen, et al., Natl. Sci. Rev. 8 (2021) nwaa160.
[29] J. Xiang, R. Zou, P. Wang, et al., Biomaterials 308 (2024) 122565.
[30] L.L. Wu, X. Meng, Q. Zhang, et al., Chin. Chem. Lett. 35 (2024) 108663.
[31] E. Gottfried, S.A. Lang, K. Renner, et al., PLoS One 8 (2013) e66987.